Deep-Sea Research I 72 (2013) 72–87

Contents lists available at SciVerse ScienceDirect

Deep-Sea Research I

journal homepage: www.elsevier.com/locate/dsri

Absolute velocity along the AR7W section in the Labrador Sea

Melinda M. Hall [a,*], Daniel J. Torres [b], Igor Yashayaev [c]

[a] Woods Hole Oceanographic Institution, 266 Woods Hole Rd., MS# 21, Woods Hole, MA 02543-1050, USA
[b] Woods Hole Oceanographic Institution, 266 Woods Hole Rd., MS# 30, Woods Hole, MA 02543-1050, USA
[c] Ocean Sciences Division, Bedford Institute of Oceanography, Fisheries and Oceans Canada, 1 Challenger Drive, PO Box 1006, Dartmouth, NS, Canada B2Y 4A2

ARTICLE INFO

Article history:
Received 20 April 2012
Received in revised form
2 November 2012
Accepted 7 November 2012
Available online 19 November 2012

Keywords:
Labrador Sea
Boundary currents
Lowered acoustic doppler current profiler
Ocean heat transport
Geostrophic velocity
Deep ocean circulation
Meridional overturning

ABSTRACT

Nearly every spring since 1990, hydrographic data have been collected along a section in the Labrador Sea known as AR7W. Since 1995, lowered acoustic doppler current profiler (LADCP) data have also been collected. In this work we use data from six of these sections, spanning the time period 1995 through 2008, to determine absolute velocity across AR7W and analyze the main features of the general circulation in the area. We find that absolute velocity fields are characterized by strong, nearly barotropic flows all along the section, meaning there is no "level of no motion" for geostrophic velocity calculations. There is strong variability from year to year, especially in the strength of the boundary currents at each end; nevertheless, combining data from.all 6 sections yields a well-organized velocity field resembling that presented by Pickart and Spall (2007), except that our velocities tend to be stronger: there is a cyclonic boundary current system with offshore recirculations at both ends of the line; the interior is filled with virtually uniform, top-to-bottom bands of velocity with alternating signs. At the southwestern end of the section, the LADCP data reveal a dual core of the Labrador Current at times when horizontal resolution is adequate. At the northeastern end, the location of the recirculation offshore of the boundary current is bimodal, and hence the apparent width of the boundary current is bimodal as well. In the middle of the section, we have found a bottom current carrying overflow waters along the Northwest Atlantic Mid-Ocean Channel, suggesting one of various possible fast routes for those waters to reach the central Labrador Sea. We have used the hydrographic data to compute geostrophic velocities, referenced to the LADCP profiles, as well as to compute ocean heat transport across AR7W for four of our sections. For all but one year, these fluxes are comparable to the mean air–sea heat flux that occurs between AR7W and Davis Strait from December to May (O(50–80 TW)), and much larger than the annual average values (O(10–20 TW)).

1. Introduction

Fundamental to understanding the world's climate system and its variability is an understanding of the ocean's participation in redistributing heat meridionally through oceanic transport and air–sea buoyancy fluxes. Intimately tied to these processes is the formation of deep and intermediate water masses that occurs as a result of deep convection driven by air–sea fluxes. It has long been recognized that deep convective processes occurring in the subpolar seas of the North Atlantic result in ventilation of the intermediate and deep water masses of the world ocean, and therefore fundamentally contribute to the meridional overturning circulation. The deepest of these water masses form in the Nordic Seas, spill over sills between Iceland and Greenland, as well as Iceland and Scotland, and flow cyclonically along the continental slope as they navigate the Irminger and Labrador Seas. In the Labrador and Irminger Seas, wintertime convection to intermediate depths results in a water mass that is characteristically cold and fresh relative to surrounding water: this process was long thought to occur only in the central Labrador Sea, but more recent studies (e.g., Pickart et al., 2002) have identified other formation regions, which produce different "flavors" of intermediate water; see also Yashayaev et al., 2007. These intermediate and deep waters depart the subpolar seas primarily as part of the Deep Western Boundary Current (DWBC). Warmer waters from the North Atlantic flow northward to replace them, and this exchange constitutes the greater part of the ocean's meridional overturning circulation MOC.

Fig. 1a schematically shows the general circulation of the Labrador Sea. A boundary current circles the rim of the basin cyclonically, comprising several components: the West Greenland and Irminger Currents flow over the continental shelf, shelfbreak and slope on the eastern side of the basin, and the Labrador Current over the shelf and slope on the western side. Waters of Arctic origin join the boundary current flow on the western side.

* Corresponding author. Tel.: +1 508 289 2599; fax: +1 508 457 2181.
E-mail address: mhall@whoi.edu (M.M. Hall).

0967-0637/$ - see front matter © 2012 Elsevier Ltd. All rights reserved.
http://dx.doi.org/10.1016/j.dsr.2012.11.005

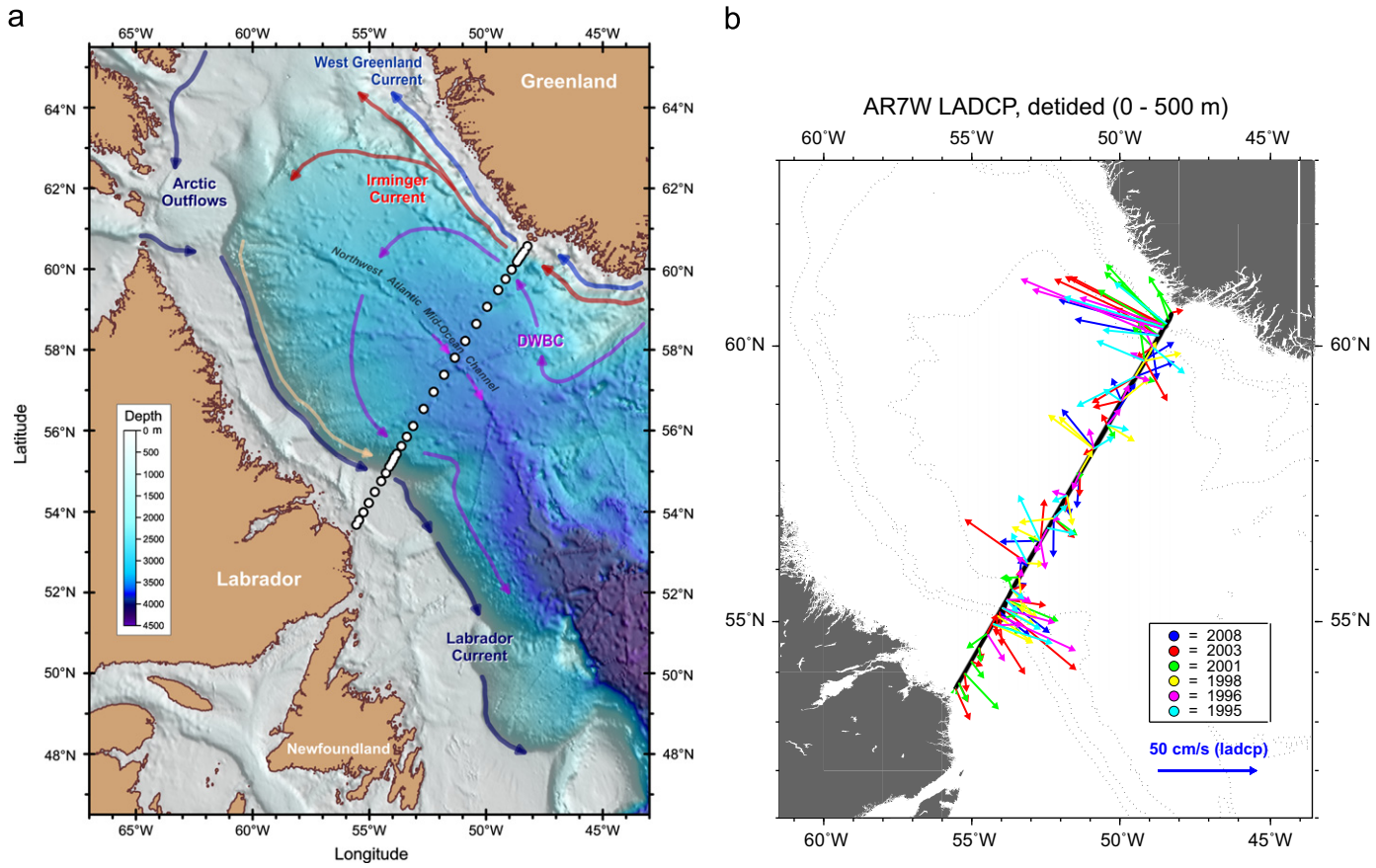

Fig. 1. (a) Schematic of circulation in the Labrador Sea; (b) LADCP vector velocities averaged over the top 500 m (or to the bottom where shallower) for sites along the AR7W line (in black). Each color represents a different year. Station positions have been projected normally onto the "standard" line (see text for more detail).

Just offshore, over the continental slope, deep-reaching currents also act as the conduit for the various water masses comprising the DWBC as they navigate the subpolar gyre. Adjacent to these boundary currents, Lavender et al. (2000), computing the absolute mean velocity field at 700 m based on trajectories of over 200 PALACE floats, found several elongated recirculation cells that together form a slow anticyclonic flow in the central basin (see, e.g., Pickart and Spall, 2007, hereafter PS2007). These structures are largely barotropic, and thus had not previously been identified in the hydrography, underlining the importance of obtaining direct current measurements. Obscuring aspects of the weaker part of the mean circulation is a spatially variable, active eddy field (Lilly et al., 2003); some of these eddies are due to boundary current instabilities and are important to restratification following deep convection in the Labrador Sea (Katsman et al., 2004). Some direct measurements do exist. Fischer et al. (2004) and Dengler et al. (2006) used several years of data from moored arrays and LADCP profiles to examine the boundary current and immediate recirculation near 53°N and 55°N on the western boundary, but their measurements did not extend into the central Labrador Sea. Likewise, Holliday et al. (2009) made limited direct measurements of the eastern boundary current near 59°N, but the data were collected over a 2-month time span, and again were confined to the boundary. What we present here, for the first time, are absolute velocity sections crossing the entire basin along AR7W, based on full-depth lowered ADCP velocity data.

Hydrographic observations have been collected annually along the line known as AR7W (see Fig. 1; also Yashayaev, 2007, and Yashayaev and Loder, 2009), which crosses the Labrador Sea in a southwest to northeast direction, and cuts through the southern edge of the primary interior convection region. These mostly springtime hydrographic cruises have been carried out primarily by Bedford Institute of Oceanography (BIO) in Dartmouth, Nova Scotia. Yashayaev (2007) has described the evolution of the Labrador Sea Water (LSW) characteristics over the years, since LSW carries a different T/S signature from year to year. Combining mean hydrography along AR7W for a 7-year period (1990–1997) with the mean flow at 700 and 1500 m as deduced from Lavender et al. (2000)'s profiling floats (1995–1999), PS2007 presented absolute velocities for the full AR7W line. The results are a useful first step to quantifying the velocity field for AR7W, but the heavy averaging required obscures instantaneously strong barotropic flows. In addition, the method implicitly assumes stationarity of the Labrador Sea circulation, an assumption that breaks down when considering the decadal and longer scales of variability in the strength of the subpolar gyre, such as described by Böning et al., 2006 and Häkkinen and Rhines (2004).

Here we present absolute velocity sections crossing the entire basin along AR7W, based on full-depth lowered ADCP velocity data collected during BIO's annual hydrographic cruises. Each section required 7–10 days to be occupied, and thus is nearly synoptic. Recognizing a valuable opportunity, scientists from the Woods Hole Oceanographic Institution (WHOI) and BIO cooperated to collect these data in what began as an unfunded effort in 1995. In late 2006, we obtained funding to support processing and analysis of the LADCP dataset, as well as the ongoing collection of data.

In this work we report on the six sections we have processed and analyzed so far, a sampling of data from 1995 to 2008. These sections illustrate the barotropic nature of velocity all along AR7W, the substantial variability of the boundary currents (and indeed the flow crossing the entire section), and what appear to

be newly observed aspects of the circulation. In Section 2 we describe the data collection and processing. Section 3 describes the velocity fields observed in the LADCP data, and in Section 4 we use the LADCP to reference geostrophic velocities from the hydrographic data, as well as examine ocean heat transport across AR7W. We conclude with a brief discussion and implications for future work.

2. Data collection and processing

Beginning in the early 1990s, scientists at BIO (Fisheries and Oceans Canada) have repeatedly occupied a line of stations that stretches from the coast of Labrador at about 53°40′N northeastward to the coast of Greenland around 60°30′N. This work began as part of the World Ocean Circulation Experiment, and has continued, more recently, as part of the World Climate Research Programme's—Climate Variability and Predictability component (CLIVAR), and the Canadian Atlantic Zone Off-Shelf Monitoring Program (AZOMP). Hydrographic data from the AR7W line have been discussed at length in several publications (e.g., Lazier et al. 2002; Yashayaev, 2007). Fig. 2(a–c) shows salinity, potential temperature, and potential density fields averaged over the six sections we use here (1995, 1996, 1998, 2001, 2003, 2008). Although the properties evolved over that time span, the large-scale patterns remain the same: the thick layer of low vertical property gradients spans the ranges of upper and deep LSW. These correspond roughly to $27.68 < \sigma_\theta < 27.74$ (kg m^{-3}) and $27.74 < \sigma_\theta < 27.8$. Below the LSW, at densities $27.8 < \sigma_\theta < 27.88$, lies a thick layer of relatively saline water, the Northeast Atlantic Deep Water, while the densest water is Denmark Strait Overflow Water. On the eastern boundary, the warm and salty Irminger Water (IW) occupies the depth range containing upper LSW over much of the rest of the section; this water undergoes modification before it can reach the western boundary, where the DWBC comprises the water masses listed above.

As noted above, lowered ADCP data have been collected along with the hydrographic data most years beginning in 1995. Some years were missed due to lack of instrument availability and others have yet to be processed due to time constraints. A single downward-facing 150 kHz broadband ADCP was used to collect all the lowered ADCP (LADCP) data for each cruise. The LADCP was typically set up to collect 16-m depth cells of single ping ensembles. Burst sampling (alternating time between alternating pings) was used to minimize effects of previous ping interference. Bandwidth and other settings were applied to maximize instrument range. The 150 kHz ADCP consistently exhibited ranges near 300 m in the upper ocean (<1500 m) dropping to around 150 m in the deeper waters (>3000 m). We therefore consider the Labrador Sea a region of very good acoustic scatter and thus conducive to good ADCP velocity measurements. The process of deriving absolute velocity profiles from raw LADCP measurements using the "shear method" was first described by Firing and Gordon (1990) and Fischer and Visbeck (1993). This method involved differentiating consecutive velocity bins within individual profiles to derive a series of overlapping shear profiles. These were then integrated to obtain a horizontal velocity profile relative to an unknown constant of integration. The profile was then referenced to bottom track absolute velocity derived from LADCP measurements within range of the bottom or ship drift over the time of the cast as determined from navigation data. The LADCP processing techniques were later further developed to allow for the use of multiple referencing constraints. The "inverse method" involves solving a set of linear equations to separate ocean and instrument velocities while applying a combination of velocity referencing constraints (Visbeck, 2002). Bottom tracking and navigation data were used as constraints for the inverse solution in most cases. Two of the cruises also used shipboard ADCP as a constraint. In a few cases, some stations did not have adequate bottom tracking to be included as a constraint. Depth of the package was usually obtained from the CTD pressure sensor (or by integrating vertical velocity if sensor was unavailable). GPS data were collected concurrently with the CTD to avoid possible clock mismatch related errors. Compass calibration of the ADCP was performed prior to each cruise. Using the inverse method with at least two referencing constraints simultaneously has been found to yield rms velocity errors of <3 cm/s (Thurnherr, 2010). The data were de-tided using a regional tidal model (Egbert and Erofeeva, 2002), which incorporates satellite altimetry observations to predict the barotropic tidal velocity. The version implemented was the 1/12° North Atlantic model, which solved for the eight tidal constituents M2, S2, N2, K2, K1, O1, P1, and Q1. The model was evaluated at each time/location associated with the midway time of each cast. Baroclinic tides are not expected to be significant on the relatively flat shelf. In deeper water past the shelfbreak, baroclinic tides are negligible.

Each time the AR7W line is occupied, an attempt is made to occupy 28 standard sites with spacing of 55 km mid-basin and 15–30 km close to the boundaries and over steep topography (Lazier et al., 2002). Additional stations may be occupied in strong mesoscale eddies or other features of interest. Inconsistent coverage of the line may occur due to inclement weather, instrument problems, or other delays. LADCP data over the broad shelf at the southwestern end of the line are available for only two occupations (2001, 2003). In 1998, dense ice coverage prevented data acquisition at the far northeastern end of the line, so the boundary current there was missed. Nevertheless, a fairly robust picture of the absolute velocity field has emerged by considering the available data from six occupations of the AR7W line.

In this paper, the primary focus is on velocity fields derived from the LADCP data alone. For the boundary currents, we compare our results with other direct measurements in nearby locations. The LADCP velocities also display a very active interior flow field, with strong depth-averaged velocities along all of AR7W. This stands in stark contrast to the nearly quiescent interior flow depicted by PS2007's mean circulation. As a secondary focus, we use the LADCP measurements to reference geostrophic velocities calculated from hydrographic data. An important result of this work is that there is no "reference level of no motion" anywhere along AR7W. Third, for several of the sections with particularly complete station coverage, we use mass conservation and a simple inverse model to estimate ocean heat transport crossing AR7W (in either direction), and put it into context with air–sea surface heat fluxes and ocean heat storage north of AR7W.

3. Results: Directly observed LADCP velocities

Fig. 1b shows the location of AR7W in the Labrador Sea, as well as vector velocities measured by the LADCP (averaged over 0–500 m, or to the bottom where the depth is shallower than 500 m) for the 6 occupations that we have processed so far. Station positions have been projected normally onto the AR7W line. This figure illustrates the salient points of the circulation: on the western end, the 0–500 m velocities in the boundary current can be as strong as 40–50 cm s^{-1}, while on the east they are even larger, as high as 60 cm s^{-1}. Just offshore of both boundary currents, velocities reverse direction over a narrow swath: these are the recirculations previously observed by Lavender et al. (2000) and discussed further in PS2007. Although the interior flows are weaker, they are by no means negligible, and since the

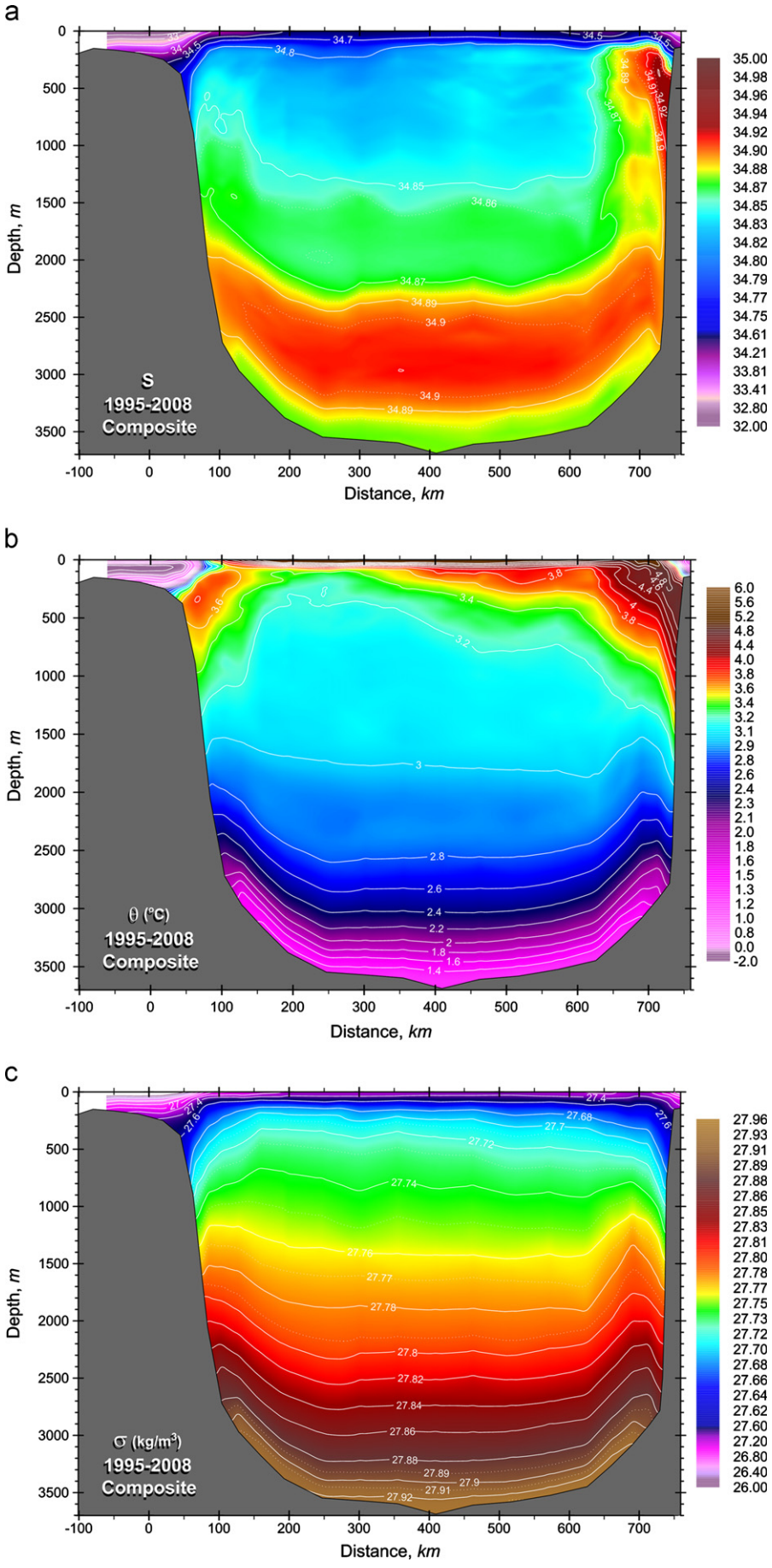

Fig. 2. Salinity (a), potential temperature (b) and potential density (c) along the AR7W section based on 6 occupations between 1995 and 2008.

flow is largely unidirectional from top to bottom (as we will see later), the vector velocities shown in Fig. 1b are generally representative of velocity direction throughout the water column.

Since we are interested in evaluating transports crossing the AR7W line, we have rotated the velocities into a coordinate system with axes along and orthogonal to the AR7W line (specifically, the rotation angle is 60 degrees in the counterclockwise direction). Although there are significant along-track velocities in locations distant from the boundaries with their steep topography, they do not contribute to cross-track flow, and are not discussed in this work. Fig. 3 shows cross-track velocity sections for all years that we are presenting here. Our sign convention is such that positive velocities, shown in pink/red, are poleward relative to AR7W (i.e., north-northwestward) while negative velocities (blue) are equatorward (i.e., south–southeastward). LADCP station locations are indicated at the top of each velocity section: typically, station spacing is 10–15 km in the boundary currents (over the steep topography) and 30–50 km elsewhere, but note that in 2001 the

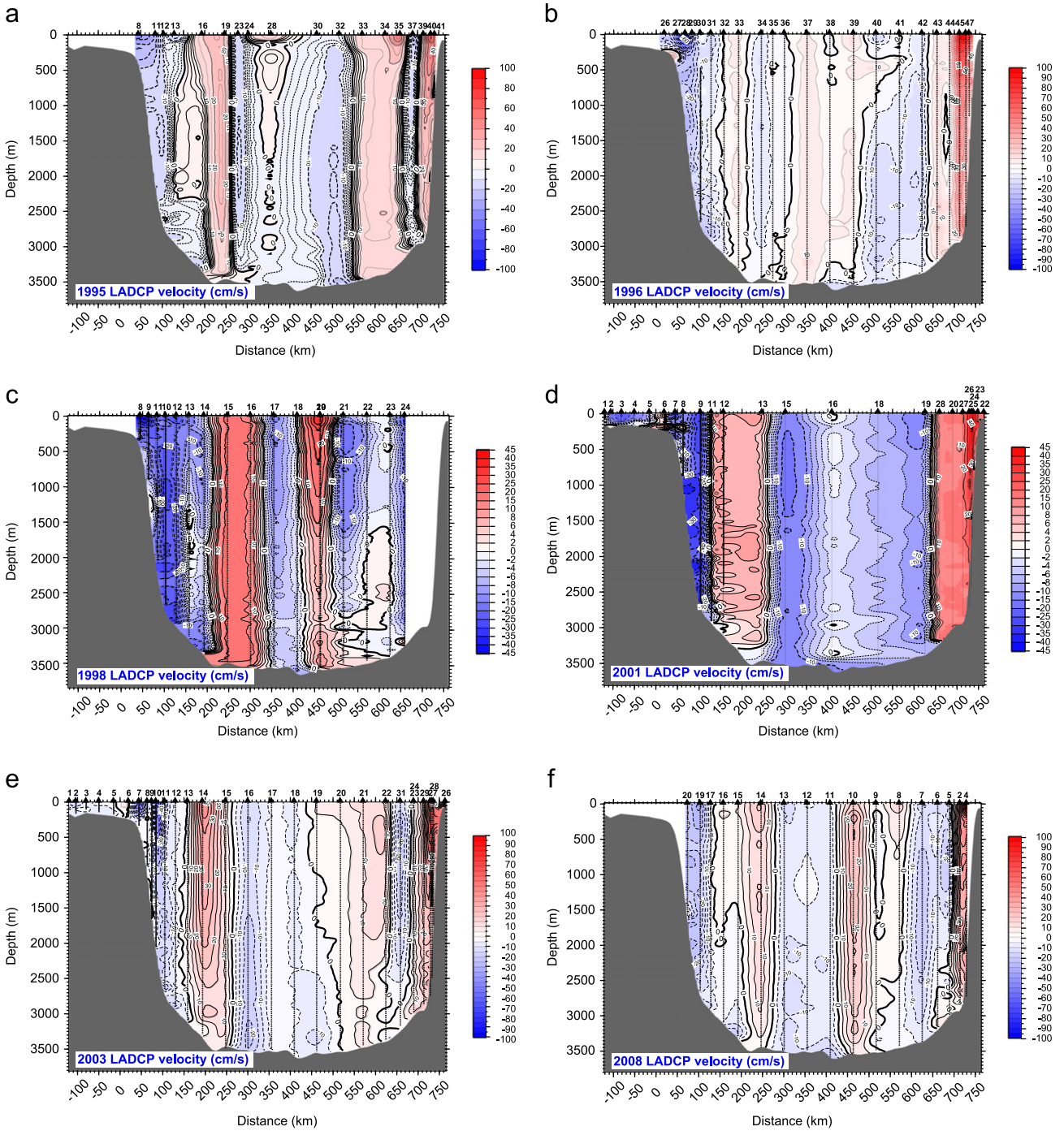

Fig. 3. Cross-track component of LADCP velocities for 6 occupations of AR7W as indicated. Southwest is on the left and northeast on the right. Velocities have been rotated 60 degrees counterclockwise to obtain along- and cross-track components (along-track not shown), and then projected onto the standard line before plotting. Positive (negative) velocities are poleward (equatorward), shown in pink (blue). Velocity scales vary.

region between 300 and 620 km was poorly sampled (station spacing around 110 km). Away from the boundary currents, station spacing is not adequate for resolving eddies, a fact that will be important later in considering mass balance.

In Fig. 3, what immediately stands out is how barotropic the flow is everywhere along the sections. Alternating bands of top-to-bottom unidirectional flow characterize the cross-track velocities almost everywhere. This may be one of the most important conclusions to come out of these observations: that, while the velocities display vertical shear, there is clearly no "level of no motion" to which geostrophic velocities could be referenced, and depth-averaged velocities tend to be strong. Boundary currents confined to the topographic slopes on either end are robust features of every occupation, though they differ in strength and extent from one section to the next. In 2001 and 2003, when spatial resolution was adequate, the LADCP data reveal a dual core of the Labrador Current (LC): inshore is the classic, shallower current, while the deep LC lies offshore, roughly over the 1500–2000 m isobath. Lazier and Wright (1993) observed and described this dual core in their seminal paper discussing annual variations in LC transport. In our observations, the inner current carries 1.6 Sv in 2001 and 3.5 Sv in 2003; the offshore current carries 5 Sv and extends down to 800 m in 2001, with 9.2 Sv occurring in 2003, when it reached about 900 m. The density contours at the western end of the section for these years (not shown) confirm the presence of a dual current core: approaching the coastline, isopycnals shallower than about 1500 m plunge downward beneath the deep expression; they then rise slightly before tending downward once more beneath the inshore LC. Other sections lacked adequate coverage to reveal the dual core.

The recirculations that are expected offshore of the boundary currents are indeed present, but display much variability from year to year, especially on the eastern end: there, a bimodality seems to exist in the current structure. In all years, there is reverse flow offshore of the eastern boundary current (EBC). However, the location at which the zero velocity contour occurs alternates between about 680–700 km and 640–650 km. When the current is tightly confined to the slope, as in 2003 and 1995, there is a distinct, narrow band of return flow just offshore of the boundary current. In other cases, the EBC is wide, and offshore lies a broader (and somewhat weaker) reverse flow. At the southwest end of the section, the western boundary current (WBC) tends to either lie entirely inshore of $X=150$ km or extend out to nearly 200 km: for 1995 and 2008, only the deeper portion does so; in 1998 the top-to-bottom current does. The region of reverse flow offshore is about 100 km wide except in 1996, but its intensity varies considerably (compare, e.g., 2001 and 2003). To formally prove that the offshore reverse flows actually recirculate some boundary current water, one would need to consider both the water properties and the along-track velocity component. However, the full basin circulation deduced from float data by Lavender et al. (2000) indicates that the countercurrents exist as parts of closed, localized cyclonic circulation.

To quantify transports and facilitate comparisons of cross-section velocities for different years, we have objectively mapped and gridded the observations. Details of this process are in Appendix. Fig. 4 shows cumulative transport curves at the western and eastern ends of the section. Each curve is pinned to zero transport at the boundaries of the plot and represents transport integration directed to the center of the line, so that the peak of each transport curve on both ends is equal to the magnitude of the measured boundary current transport. Successive curves are offset by 15 Sv, because they would otherwise coincide too closely for details to be visible. Some of the curves extend into the recirculation regions: the curves are terminated where station spacing becomes too large (as a rule larger than 30 km). The transport over the southwestern shelf,

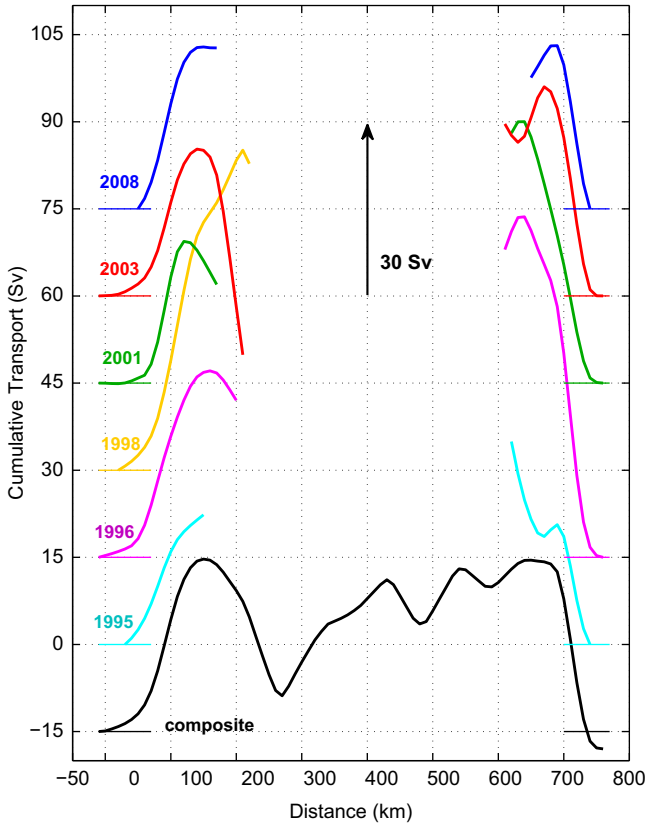

Fig. 4. Cumulative transport curves for the boundary currents in all years (colors correspond to those of vectors in Fig. 1). At both ends, absolute boundary current transport is integrated from zero at the limits of observation, X_{min} or X_{max}, towards the interior. Also shown is the entire cumulative transport curve for the composite velocity field (black curve). For comparison with the boundary current curves, regions of positive slope on the composite curve correspond to equatorward velocity and vice versa. Units are Sv ($1\ Sv=10^6\ m^3\ s^{-1}$). On the west, curves start at -10 km or else at roughly the first station position; likewise, on the east, they terminate at 760 km or the last station position (move this to caption).

omitted in Fig. 4, is 1.5–1.9 Sv of equatorward flow, based on the two years (2001, 2003) for which we have LADCP data there.

Note that in Fig. 4 the transport curves at the eastern end reach higher levels than their counterparts on the west in 1996, 2001, and 2003. No data were available at the eastern end for 1998. In 1995, EBC transport integrated beyond the narrow band of reverse flow occurring at about 690 km also exceeds WBC transport. For 2008, comparable transport is computed at both ends, but the section terminates at 730 km; comparison with 2001 and 2003 suggests that some 3–4 Sv of transport occurs onshore of 730 km. Examination of the hydrographic property sections (Fig. 2a–c) shows that the warm, saline Irminger Current water entering the basin on the eastern end does not make it around the perimeter to the western boundary current, suggesting that much of the transport difference between the eastern and western boundary flows is associated with loss of the warmer water into the central Labrador Sea (e.g., through instability processes), where it undergoes heat loss to the atmosphere; we return to this idea in Section 4.1.

Table 1 shows western and eastern boundary current transports for each occupation: these differ somewhat from values implied in Fig. 4 because we have considered only the poleward (or equatorward) flow inshore of the zero velocity contour on each boundary, with the exception of waters over the inner shelf at the southwestern end. In order to compare with other authors'

Table 1
Western (top, WBC) and eastern (bottom, EBC) boundary current transport estimates based on LADCP measurements for 6 occupations of AR7W, year indicated in top row. Transports are broken down into 4 density classes as indicated, determined from hydrographic data collected concurrently with the LADCP data. Mean transports are shown, as well as transports for the composite velocity field; F refers to Fischer et al. (2004), and D1 and D2 to Dengler et al. (2006), who divided results into an earlier (1996–1999, D1) and later (2001–2005, D2) time period. For EBC's, results in parentheses show a different division among the top two density classes, for comparisons with Holliday et al. (2009). All WBC transports are equatorward (southeast) and all EBC transports are poleward (northwest).

WBC	1995	1996	1998	2001	2003	2008	Mean	Comp.	F	D1	D2
$\sigma_\theta < 27.74$	11.4	13.6	20.3	9.2	16.0	17.2	14.7	14.5	12.3	12.0	15.5
$\sigma_\theta < 27.8$	10.0	9.9	18.6	9.6	3.9	6.0	9.7	8.5	10.7	9.9	9.4
$\sigma_\theta < 27.88$	3.4	5.9	11.3	5.7	4.4	7.8	6.4	5.6	9.4	7.3	9.8
$\sigma_\theta > 27.88$	2.4	2.5	5.3	0.3	1.3	2.5	2.4	2.1	5.3	2.6	3.9
Total	27.3	31.9	55.5	24.8	25.6	33.5	33.1	30.7	37.7	31.8	38.6
EBC	1995	1996	1998	2001	2003	2008	Mean	Comp.		Comp.	H
$\sigma_\theta < 27.7)$	(6.1)	(21.7)	n/a	(12.8)	(16.7)	(15.8)	(14.6)			(14.0)	14.1
$\sigma_\theta = 27.7–8)$	(12.2)	(20.3)	n/a	(20.9)	(11.3)	(8.7)	(14.7)			(12.2)	20.0
$\sigma_\theta < 27.74$	9.6	27.4	n/a	22.4	20.6	19.9	20.0			18.8	
$\sigma_\theta < 27.8$	8.7	14.7	n/a	11.3	7.5	4.5	9.3			7.4	
$\sigma_\theta < 27.88$	3.3	11.4	n/a	8.9	6.4	3.2	6.7			5.5	12.0
$\sigma_\theta > 27.88$	0.4	3.7	n/a	2.5	1.9	1.0	1.9			1.8	7.7
Total	22.0	57.2	n/a	44.2	36.4	28.6	37.9			33.5	53.8

estimates, we have used the CTD data to determine transport in 4 density layers: the three deepest layers roughly correspond to Labrador Sea Water (LSW), Northeast Atlantic Deep Water, and Denmark Strait Overflow Water. The top layer deepens considerably from 1995 to 2003, as very little deep winter convection occurred after 1994 (Yashayaev, 2007). Results from other studies for the western boundary in nearby locations are included in Table 1.

Boundary current transports range from as low as 22 Sv to as high as about 55 Sv, for both east and west; for 1996, 2001 and 2003, higher transport values occur in the eastern boundary currents, as in Fig. 4. The low EBC transport for 1995 is due to including only those waters inshore of the narrow reverse flow. Although EBC transport in 2008 may again be underestimated, other evidence suggests that no loss of IW from the boundary current occurred in 2008: Yashayaev and Loder (2009) found no sign of cooling of Irminger Current water from the eastern to the western boundary for the 2008 section, suggesting no loss of IW from the boundary current. Strong variability in boundary current transports is not surprising: Fischer et al. (2004), using data from a moored array, determined that short-term (i.e., intraseasonal) variability introduced the largest source of uncertainty in their mean WBC flow at 53°N, with a range of 15–35 Sv for $\sigma_\theta > 27.74$ (see also Fischer et al., 2010). This variability swamps seasonal and interannual variability, estimated from satellite data to be O(5–6 Sv) each (Han and Tang, 1999, 2001), and is also much larger than instrument errors would introduce in the calculation: the area of the boundary current with $\sigma_\theta > 27.74$ is about 1.74×10^8 m^2. Thus, the measurement error of < 3 cm s^{-1} would lead to a maximum transport error of 5.2 Sv.

Fischer et al. (2004) and Dengler et al. (2006) also present time averaged values of WBC transport; because of the spread in our individual section estimates, we compare these with our mean transport values. Our mean WBC transport (33.1 Sv) is lower than their values (37.7 Sv for Fischer et al. 2004; 35 Sv for Dengler et al., 2006), though for their early reporting period, 1996–1999, Dengler et al. (2006) found a value of 31.8 Sv. The boundary current throughput computed by PS2007 is 28.5 Sv. The mean transport that we present also shows a somewhat different distribution of transport in density classes than either Fischer et al. (2004) or Dengler et al. (2006); somewhat puzzling is that we consistently find less (7–8 Sv) in the dense water ($\sigma_\theta > 27.8$) than do the other studies (12–15 Sv). Such a large amount cannot be accounted for merely by instrument error or undersampling. This part of the current is approximately 80 km wide and 1000 m thick, so a systematic bias of more than 6 cm s^{-1} would be required to account for 5 Sv. But, as noted above, the LADCP measurements are accurate to < 3 cm s^{-1}. It is also possible that the LADCP velocity profiles missed the peak velocity in the deep boundary current. For example, two stations separated by 30 km might measure peak velocities of 20 cm s^{-1}. If the true maximum were 40 cm s^{-1}midway between the stations, and extended over 500 m depth, transport would be under-estimated by 1.5 Sv. Thus, the maximum error due to a combination of measurement error (about 2.5 Sv) and under-sampling (1.5 Sv) in this case would be about 4 Sv, less than the actual measured difference. We therefore conclude that the measured difference is real, and due to temporal variations in the current.

Few observations are available for comparison with our EBC transports. Holliday et al. (2009) report on an August–September 2005 CTD and LADCP survey of the currents around the tip of Greenland, and include a section in the Labrador Sea about 150 km to the southeast of AR7W, where the shelf and slope are somewhat broader and less steep than they are in our section. They used a different isopycnal to divide the top two layers: Table 1b shows Holliday et al. (2009)'s and our transports for the

EBC in these layers. The differences in both the layer and total transports are large, but we speculate that time variability has more to do with this than factors such as topography or the presence (or not) of recirculations. Our transport values for the water denser than σ_θ=27.8 are comparable to those that Holliday et al. (2009) found for their Irminger Sea and Eirik Ridge sections, but only half of their value for the Labrador Sea section. In accounting for the differences between the sections in their own work, they concluded that both recirculation and time variability (in particular, "synoptic errors introduced by mesoscale activity") are responsible for the difference. Given the broad range of EBC transports in all the layers for the different occupations of AR7W, and the fact that they come from a different time of year than the Holliday et al. values, we should probably not expect the different estimates to agree. Furthermore, the bimodality in the current structure at the eastern end is associated with transport differences: lower transports occur for the case of a more confined, narrower EBC. Mean boundary current transports in Table 1 show 5 Sv more in the EBC than in the WBC, nearly all of which occurs in waters lighter than σ_θ=27.74. This result is consistent with the hypothesis that much of the warm and salty Irminger Water entering the Labrador Sea from the southeast corner of the basin leaves the boundary current instead of circling the basin and exiting on the western side. Some of this Irminger Water ends up in the central Labrador Sea due to instabilities of the boundary current (e.g., Katsman et al., 2004), and some continues northward into Baffin Bay (Cuny et al., 2005, note a 1.2 Sv northward flow through Davis Strait at its eastern end).

Myers et al. (2007) used historical data along three sections in the West Greenland Current to study variability of the IW there. For the time period 1995–2005, they found 4.9 Sv at the Cape Farewell Section 3.1 Sv at Cape Desolation, and 0.8 Sv at Paamiut (going from south to north, i.e., downstream in the West Greenland Current). The Cape Desolation section lies just north of AR7W, and the loss of 2.3 Sv of IW downstream appears to be roughly consistent with our results. Such a comparison is problematic, however, for several reasons: first, their results are based on geostrophic velocities relative to 700 dbars, with barotropic adjustments of 5–7 cm s^{-1}. Velocities shown in Fig. 3 at this depth on the eastern end of AR7W are considerably higher. Second, the Paamiut section lies north of the recirculation region, so a downstream decrease in northward flowing IW is expected without necessarily implying loss to the center of the Labrador Sea. Third, our results hold for water lighter than σ_θ=27.74, and generally this isopycnal lies deeper than 700 dbars, the limit of their calculation, so the estimates are not entirely comparable.

3.1. Composite velocity field

Fig. 5a shows a composite velocity section based on the 6 years of LADCP data we present here. To construct it, individual sections were mapped with 20-km horizontal and 25-m vertical smoothing scales; we assign NaN's to grid points that are too distant from the nearest stations to allow an estimate. We then averaged these 6 sections, including only the real (non-Nan) values at each grid

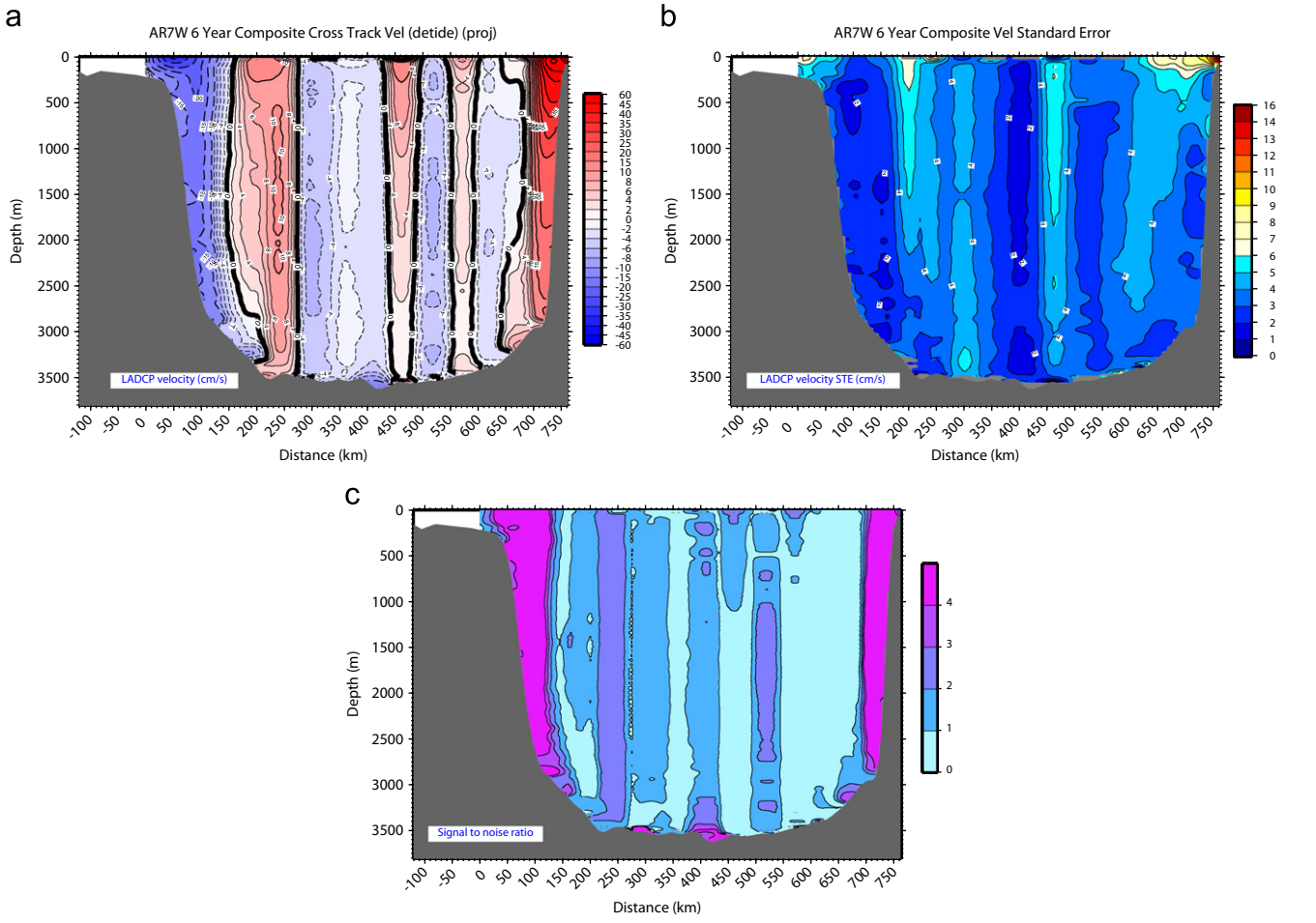

Fig. 5. (a) Composite cross-track velocity section based on LADCP profiles from 6 occupations of AR7W (see text); (b) standard error and (c) signal to noise ratio (SNR), computed as described in text.

point; the number of sections used in each grid point gives the degrees of freedom N for the estimate. A standard error SE of the mean is computed equal to the standard deviation divided by $\sqrt{N}$ (Fig. 5b). This is compared with the mean velocity to obtain a signal-to-noise ratio, shown in Fig. 5c.

In the western boundary current, the composite largely smoothes over the double core of the Labrador Current; at the eastern end, it splits the difference between the two modes of recirculation noted above, and the result is a rather weak and confined region of reverse flow between about 600 and 650 km. The recirculation offshore of the WBC is more robust (both stronger and wider), reflecting the consistency seen in this feature from one occupation to the next. Comparing our composite with the absolute velocity section of PS2007 (their Fig. 3a), we find that the two are qualitatively similar but quantitatively different. Both sections show strong boundary currents at either end of AR7W, with some offshore recirculation. The interior in both is filled with top-to-bottom bands of alternating velocity. However, in our composite the boundary currents are more confined to the continental slope, with the zero velocity contour occurring about 50 km farther onshore than in PS2007. Maximum current strength in the boundary currents is comparable for the two sections, but interior flows in PS2007's depiction are much weaker than ours, by a factor of about 5. Because of the quiescent nature of their interior velocities, PS2007 were able to clearly identify the boundary current "throughput" from any recirculating flow. Such a separation is not possible for our sections, owing to the vigor of all interior flow.

The cumulative transport curve for the composite field is shown in Fig. 4 (black curve). Like the individual occupations, the composite field has a stronger eastern than western boundary current; the curve does not terminate at zero, indicating that a net of 3 Sv flows north across AR7W; over the southwestern shelf (not shown), 1.7 Sv flow south, partly balancing this transport. To the north of AR7W, the Labrador basin is closed except at Davis Strait and Hudson Strait. Curry et al. (2011) report an annual net southward flow through Davis Strait of 2.3 Sv (closer to 4 Sv during spring). Measurements from Drinkwater (1988) imply negligible net transports through Hudson Strait. Our result combined with the mean flow through Davis Strait implies a net convergence of 3.6 Sv in the volume between AR7W and Davis Strait, which is impossible, in the absence of sea level rise. It would be a mistake to attach too much importance to this imbalance since, as we have noted, a typical survey takes about a week. Additionally, the 55-km station spacing over the interior is too large to resolve mesoscale eddies, which may bias the transport. The contribution of river runoff to mass balance is orders of magnitude smaller (see Section 4.1).

In Fig. 5c, there are large swaths of the section where the SNR is less than one: these areas occur in the interior portions where sampling was sometimes sparse and the location of the zero velocity contour varied from section to section. The boundary current signals are strong, as would be expected. At the eastern end, the varying location of the recirculation leads to a low SNR, while the western recirculation has a robust signal around 200–250 km. The region of low SNR between this location and the western boundary current is the result of the varying location of the offshore edge of the WBC.

Boundary current transports for the composite section are also given in Table 1: these values are slightly lower than for the means of the individual years, because the regions of positive-only (or negative-only) velocity are smaller, since the composite inherently smoothes over extremes. For the composite velocity field, transport of water lighter than $\sigma_\theta = 27.74$ decreases from 18.8 Sv in the EBC to 14.5 Sv in the WBC, a change of 4.3 Sv. Based on the values of SNR in the boundary currents, transport errors due to sampling are on the order of 20% for the western boundary (± 6 Sv) and 25–30% for the eastern boundary (± 8–10 Sv). Transport errors due to instrument error are expected to be the same as or smaller than those for individual sections (± 2.5 Sv, see above), since the composite field is essentially a smoothing process.

Of particular interest in Fig. 5a is a bottom-intensified southeastward flow centered more or less over the trench near 400 km; high values of the SNR in Fig. 5c at this location indicate that it is a robust feature. Indeed, the same feature can be seen in the cross-track velocity for at least 3 of the individual sections, in 1996 (Fig. 3b), 1998 (Fig. 3c) and 2008 (Fig. 3f); in 1996, the signal is even stronger when viewed in geographical coordinates, as a southward flow. In 2001, though not obvious in cross-stream coordinates, the current is visible in a bottom intensified southward flow. The flow was not detected in the 2003 velocity section, and in 1995 no LADCP data were collected at that location. Yashayaev and Dickson (2008) have noted the rapidity with which signals of hydrographic change in the densest overflow waters, entering the Labrador Sea around the southern tip of Greenland, can spread to the interior of the basin. This trench along the northwest–southeast axis of the Labrador Sea has been termed the Northwest Atlantic Mid-Ocean Channel (NAMOC) and has been recognized as a turbidity current pathway by petrologists (e.g., Chough and Hesse, 1980; Chough et al., 1987). We hypothesize that it also provides a pathway for Denmark Strait Overflow Water to reach the central Labrador Sea with little delay. Another small channel crosses the NAMOC in a direction very nearly aligned with the AR7W track, the two intersecting at one of the standard AR7W stations (around 410 km in Fig. 3): this may account for the varying direction of the bottom flow. From the composite velocity section, we estimate that roughly 0.2 Sv of transport occurs in this current, i.e., as much as 10% of the Denmark Straits Overflow crossing the Greenland–Iceland Ridge. We believe that these are the first direct measurements of this abyssal current. At this time there is scant data for examining this feature in more detail, but further investigation of its vertical and horizontal structure, as well as seasonal and longer-term variability, is warranted.

4. Comparison with geostrophic velocities

One goal of collecting the LADCP data was to provide reference level information for geostrophic velocity calculations. Geostrophy inherently smoothes over small vertical scales, as dynamic height is an integral of specific volume anomaly, and horizontal spatial scales can be resolved only to the station spacing. It also suppresses the ageostrophic velocity components that LADCP data may include. Because the dynamic method yields only baroclinic velocities, we expect this geostrophic velocity field to evolve over the baroclinic time scale – that is, more slowly than the barotropic velocities may change – and therefore to be worthwhile examining if we seek to understand the larger scale flow crossing AR7W. However, since the interior of the section displays substantial bottom velocities (Fig. 3a–f), the LADCP data are indispensable for estimating the absolute geostrophic velocities, as opposed to bottom-relative ones.

Geostrophic velocities have been calculated relative to the deepest common level (DCL) of each station pair, with constant velocity below that (i.e., bottom velocity equals zero before any barotropic contribution is added). To compare this profile with the LADCP data, we average the two LADCP profiles from the two CTD stations used in computing the geostrophic profile, again down to the DCL for the two stations. We then take the depth average of each of these profiles above the DCL, and the offset is taken to be the reference velocity to add to the geostrophic

profile: in our case, it is also the bottom velocity for the geostrophic profiles. This approach works especially well where the vertical shear is strong, i.e., in the boundary currents: Fig. 6a presents examples in the eastern boundary current for 1995, and the western boundary current for 1996. In the interior, vertical shear is often weaker in the geostrophic profile, and though it is not obvious that averaging two LADCP profiles should yield a similar shear, the comparison between the average LADCP profile and the geostrophic velocity is still often very good (Fig. 6b). Frequently, the worst comparisons occur when the 2 LADCP profiles from the individual stations differ substantially (Fig. 6c), suggesting that the profiles come from different features of the flow. For consistency, however, we apply the same methodology over all station pairs. This method has been used successfully before (Joyce et al., 2001; Hall et al., 2004) under similar circumstances, i.e., a trans-basin section crossing boundary currents. Because velocities measured by the ADCP include ageostrophic effects, especially in the upper layers, we have not tried to incorporate the vessel-mounted ADCP data into the reference level calculations. Rather, it is important to compare shear over the entire water column, which is more likely to reflect the geostrophic part of the velocity.

Fig. 7 shows the geostrophic velocity for 2008 referenced to the bottom/DCL (Fig. 7a) and with the LADCP-based reference velocity added in (Fig. 7b). By comparison with the LADCP velocities for 2008 (Fig. 3f), there is less vertical structure in the interior of the flow for the geostrophic section. Nevertheless, the transport is dominated by contributions from the reference velocities, so the cumulative transport curve for LADCP-referenced geostrophic velocity is quite similar to that for the LADCP alone (Fig. 7c): this is true of all the sections we have examined, and is to be expected, as it is the result of the vigorous interior velocity field revealed by the LADCP. Note, however, that even in the boundary currents the bottom-relative geostrophic velocities are much weaker than LADCP velocities, owing to strong barotropic contributions. For all

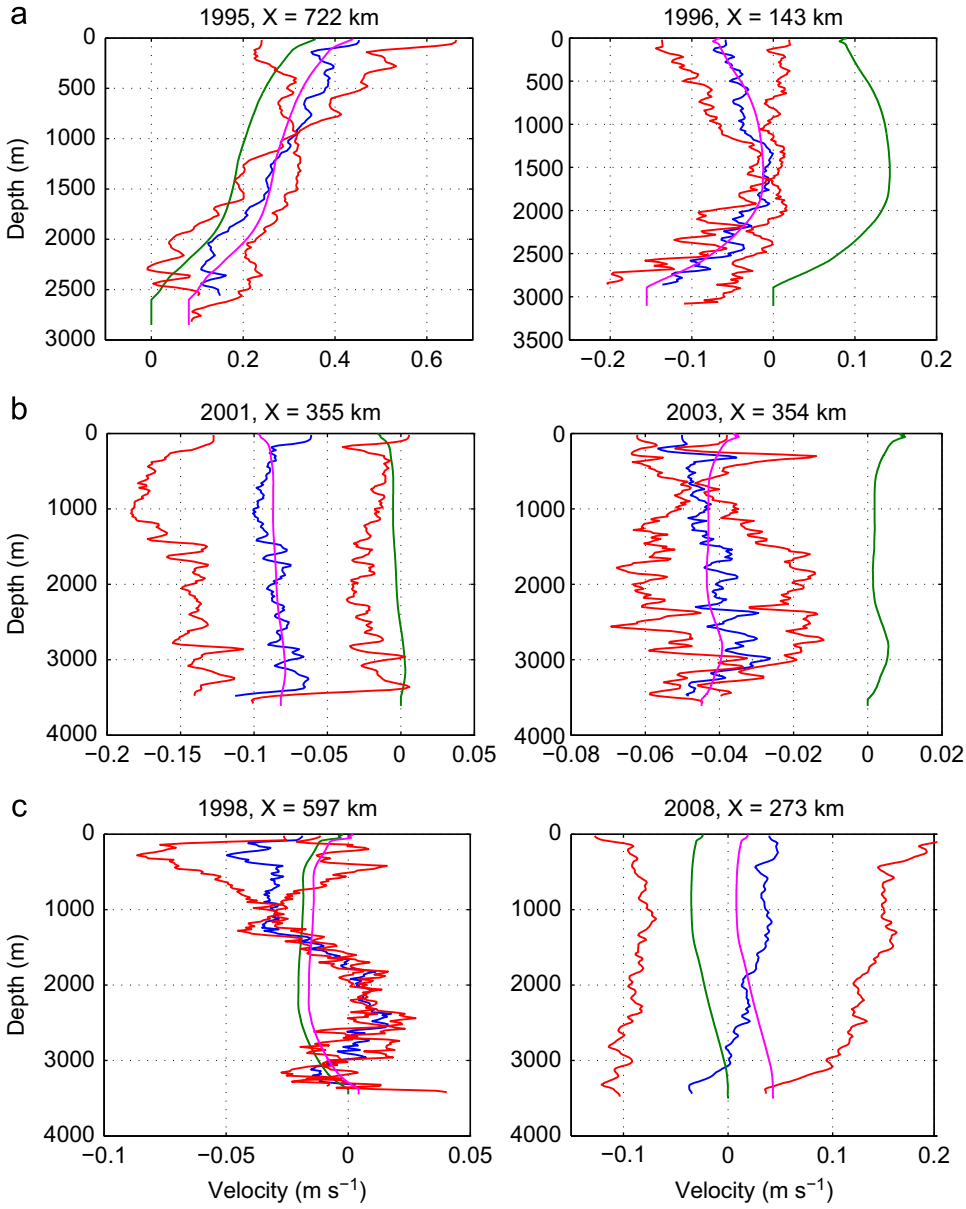

Fig. 6. Comparisons of LADCP and geostrophic shear for 3 cases: (a) strong shear, good agreement; (b) weak shear, good agreement; (c) poor agreement, resulting from 2 substantially different LADCP profiles. Red profiles are LADCP velocity from each station in the pair; blue is the average LADCP velocity; green profile is bottom-relative geostrophic velocity; mauve profile is geostrophic velocity adjusted to mean LADCP profile.

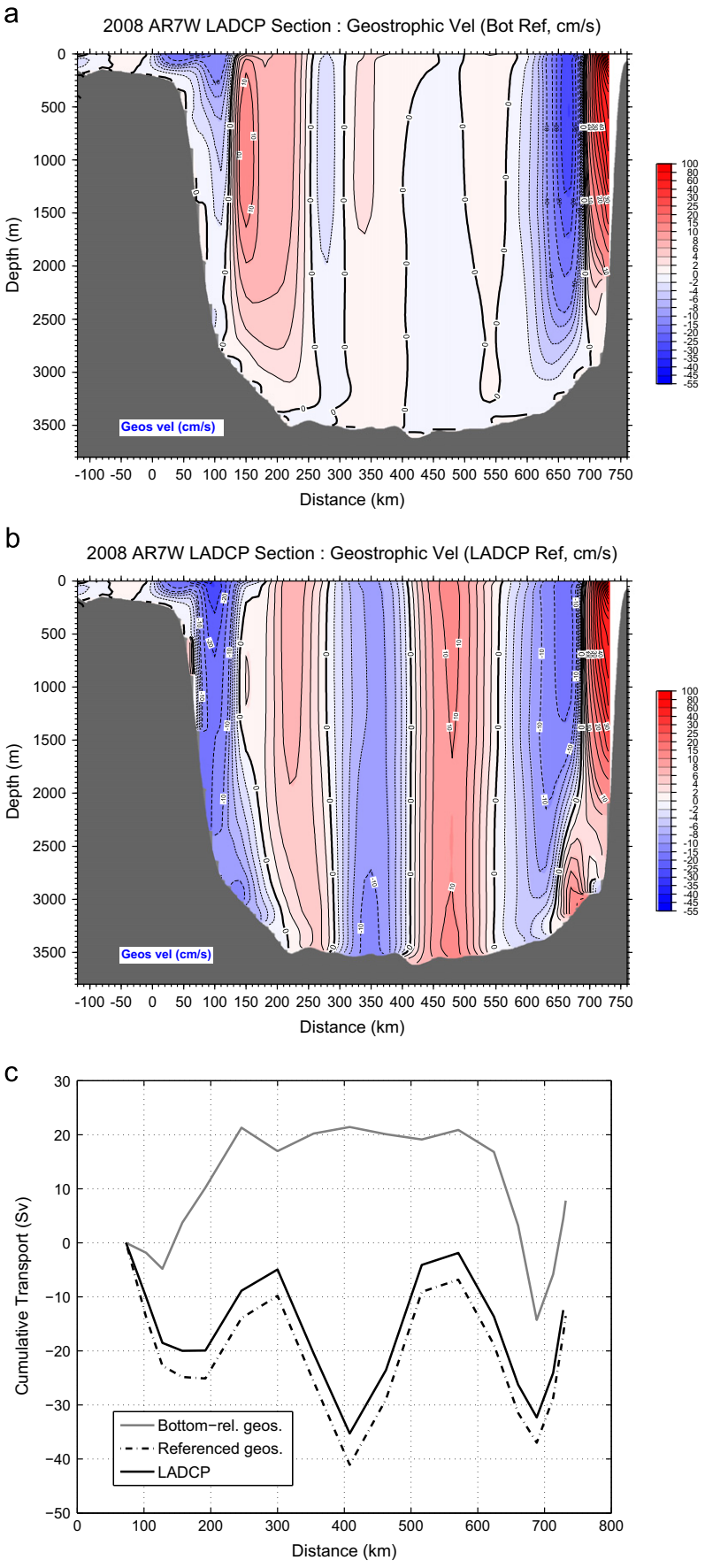

Fig. 7. (a) 2008 geostrophic velocity referenced to bottom/DCL; (b) same, but now with LADCP-referenced velocity added in; (c) cumulative transport curves for bottom relative geostrophic velocity, LADCP-adjusted geostrophic velocity and straight LADCP velocity (component normal to AR7W). Here, positive slopes correspond to poleward velocity.

years, the cumulative transport curve for the bottom-relative geostrophic velocity has a shape similar to that shown for 2008 in Fig. 7c; the cumulative transport curves for LADCP-referenced geostrophic velocity closely resemble the full-section cumulative transport curves from the LADCP alone (not shown).

It is instructive to compare our results with Kieke and Rhein (2006), who used historical hydrographic data to examine variability of overflow transports in the Irminger and Labrador Seas. Due to the sparsity of direct measurements, they used 1400 dbars as a reference level, since it is in the weakly stratified LSW. They concluded that there is a baroclinic cyclonic circulation of 7–8 Sv in the Labrador Sea; we find 4.9–8.4 Sv of southward flowing overflow waters ($\sigma_\theta > 27.8$) at the western boundary, with a mean of 6.8 Sv. However, in the western recirculation zones of AR7W, the LADCP velocities show shear that is either negligible or the same sign as that in the boundary current itself (Fig. 3a–f). Thus, the southward transport of overflow waters calculated in this way includes some recirculation, which should be going northward. Indeed, there is no way to determine the boundary between the boundary current and the recirculation based on baroclinic velocities alone. At the eastern boundary, a 1400-dbar reference level gives deep velocities that are the wrong sign in both the boundary current and recirculation, which explains why the eastern end of Kieke and Rhein's (2006) cumulative transport curves (their Fig. 5) suggest southward flow right next to the eastern boundary.

4.1. Ocean heat transport

The Labrador Sea Deep Convection Experiment was a large collaborative effort that began in the late 1990s to directly observe deep convection and use the results to guide modeling efforts to better understand the physics of this process (Lab Sea Group, 1998). The focus was on understanding the interplay between buoyancy exchange with the atmosphere, convergence of warm waters into the region, the role of eddies in redistributing heat, and the export of convected water masses via the boundary currents. A number of results have emerged from this experiment. Pickart et al. (2002) identified two distinct regions of convection based on hydrographic data collected on a February–March, 1997 cruise. The first regime was offshore of the boundary currents, in deep water: this is the classical LSW ($LSW_{1987\text{-}94}$ in Yashayaev et al., 2007), formed when cold air masses coming off the North American continent in winter lead to strong air–sea buoyancy fluxes, which in turn destabilize the water column and lead to deep convection. In addition, convection was observed to occur directly into the western boundary current, shoreward of the 3000-m isobath; this water mass was warmer, saltier and lighter than classical LSW. Pickart et al. (2002) also noted that convection did not occur in the eastern Labrador Sea, probably owing to the stabilizing influence of a freshwater cap emanating from the eastern rim current; nor did it occur farther north than AR7W, again owing to higher ambient stratification, in this case due to eddies propagating westward from the eastern boundary.

Brandt et al. (2007) used a model of the subpolar North Atlantic to examine and distinguish between transformation and ventilation rates in the presence of moderate convection; they found a transformation rate 6.8 Sv into the density class $27.74 < \sigma_\theta < 27.83$, which includes LSW but also overflow waters. More typical estimates of LSW formation range from 2 to 4 Sv (Khatiwala et al. 2002); Clarke and Gascard (1983) found that 10^5 km^3 of LSW was formed in 1976 (3.2 Sv, annualized). They also found rapid export of recently transformed water via the deep Labrador Current.

Katsman et al. (2004) used a model to look at the restratification process following deep convection, and concluded that Irminger Eddies, spun off from the boundary current on the eastern side of the Labrador Sea, were important to this process. Straneo (2006) investigated the processes involved in deep convection and restratification in the central Labrador Sea, using data from two different time periods. She noted that the source of heat for the central Labrador Sea is warm Irminger Water that is "advected into the basin, between 200 and 700 m, by the cyclonic boundary system." She further noted that this region experiences net surface heat loss to the atmosphere, balanced by a "convergence into the region due to the oceanic circulation," but she could not establish a correlation between these two mechanisms. Here we take a different approach, and consider the poleward ocean heat transport across AR7W, the divergence or convergence of heat in the oceanic volume lying between AR7W and Davis Strait, and the surface heat loss to the atmosphere integrated over the entire area of the Labrador Sea north of AR7W. This method integrates over regional scale processes to give a larger-scale picture of the contribution of the Labrador Sea to the meridional overturning circulation.

In order to make a meaningful estimate of ocean heat transport into a closed basin, it is necessary to balance mass transport (Hall and Bryden, 1982). In theory, the net mass transport crossing the AR7W line must balance any net flow through Davis Strait, because: (1) PS2007 have shown that the Ekman contribution to cross-track mass transport is small; (2) at Hudson Strait a northwest flow into the Hudson Bay approximately balances the southeastward outflow, though the properties of the in- and out-flowing waters differ (Drinkwater, 1988); and (3) contributions from freshwater sources are several orders of magnitude smaller than transports crossing AR7W (Khatiwala et al., 2002). Curry et al. (2011) reported on mass, heat and freshwater fluxes crossing Davis Strait based on a one-year deployment (September, 2004, through August, 2005) of 14 moorings with instrumentation measuring velocity, temperature and conductivity. They found annual mean mass, heat, and freshwater fluxes of -2.3 Sv, 20 TW, and -116 mSv (heat flux was calculated relative to 0° C and freshwater flux relative to 34.8). Peak mass transport occurs in June and is about 4 Sv southward; in that month heat flux is minimal, about 5–10 TW poleward.

Two points allowed PS2007 to make a meaningful calculation of ocean heat flux crossing AR7W. First, they assumed that the Davis Strait flow, coming from depths less than 600 m (the sill depth) and densities mostly lighter than $\sigma_\theta < 27.55$, must occur inshore of the 700-m isobaths (thus, outside their area of coverage). Second, their section represented a mean flow over a period during which the hydrographic properties were fairly steady. However, the six sections we examined span a longer period of time, during which properties evolved significantly, as the strong overturning of the mid-nineties gave way to a long period of meager winter overturning. Thus, rather than trying to estimate a mean ocean heat transport across AR7W for the period 1995–2008, we have explored the heat flux calculation for individual sections, limiting ourselves to the 4 sections that had end-to-end coverage in at least the hydrographic data: 1995, 1996, 2001 and 2003.

Because our LADCP-referenced geostrophic velocities do not in general conserve mass, we have run an inverse calculation (following Joyce et al., 2001) requiring that the circulation balance mass to within 0.5 Sv overall; it must also balance mass within certain limits for 6 density layers (for $\sigma_\theta > 27.8$, the amount is 0.3 Sv: see Table 2). In formulating the inverse, we add the Davis Strait transport to the uppermost density layer. The calculation yields velocity adjustments for each station pair, which generally are small relative to the overall velocity profile for a given station pair, and therefore do not change the character of the velocity sections appreciably. Fig. 8 demonstrates the effect of the inverse procedure on the cumulative transport curve for 1995: the maximum velocity adjustment for any pair of stations in the

Table 2
Allowed mass transport imbalances for given density layers when running inverse. The totals do not include the Davis Strait transport, which is included in the uppermost layer before the inverse is applied.

Density range	Variance
$\sigma_\theta < 27.55$	2 Sv
$27.55 < \sigma_\theta < 27.71$	1 Sv
$27.71 < \sigma_\theta < 27.74$	1 Sv
$27.74 < \sigma_\theta < 27.776$	1 Sv
$27.776 < \sigma_\theta < 27.8$	1 Sv
$\sigma_\theta > 27.8$	0.3 Sv
Total (top to bottom)	0.5 Sv

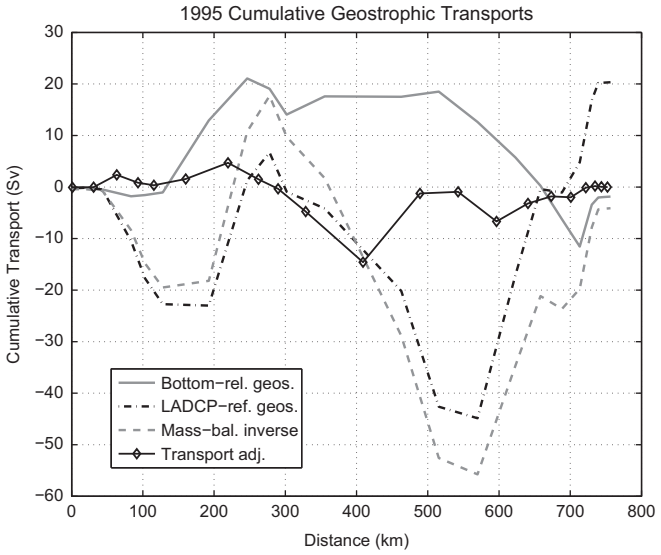

Fig. 8. Cumulative transport curves showing the effect of the inverse calculation for 1995: shown are the curves for bottom-relative geostrophic velocity (solid gray line); LADCP-referenced geostrophic velocity (dash-dotted black line); the curve for the mass-balanced inverse solution (gray dashed line); and the individual transport adjustments (not cumulative) for each station pair, calculated from the inverse.

Table 3
Ocean heat transport crossing AR7W for different years (units are terawatts), based on the LADCP-referenced geostrophic velocity fields to which an inverse has been applied to balance mass transport. Three different cases are considered for transport coming south through Davis Strait (DS; see text for more detail). Positive transports are poleward.

Year	DS = −4 Sv	DS = −2.3 Sv	No DS flow
1995	0.10	11.5	32.2
1996	76.9	89.4	125.8
2001	50.6	66.2	92.3
2003	50.8	68.0	90.7

center of the basin is 3.7 cm s^{-1}, at 409 km. This coincides with a region of low horizontal resolution, so that the mass transport adjustment at that location is much larger than anywhere else on the section (solid black line with diamonds). Overall, the adjustment systematically brings the cumulative transport curve to −4 Sv, the amount required to accommodate the Davis Strait inflow from the north.

For the four sections examined herein, we have considered three different cases, and the results are summarized in Table 3. In the first case (column 2 of Table 3), we have imposed a Davis Strait transport of 4 Sv southward. That corresponds to the measured transport for June in Curry et al. (2011); since the AR7W sections were occupied in spring, this choice of DS transport seems most logical. However, we have also considered two other cases, shown in columns 3 and 4 of Table 3: in column 3 are the results for the case of Davis Strait flow of −2.3 Sv, the annual average from Curry et al. (2011); and in column 4 we show results for the heat flux when the Davis Strait flow is completely omitted. For all cases, the computed heat flux is by far smallest for 1995 and largest for 1996. The sections made in 2001 and 2003 yield very similar results. For all four years, the heat flux in column 2 (Davis Strait flow of −4 Sv) is 10–15 TW lower than that in column 3 (Davis Strait flow of −2.3 Sv; 1 TW = 10^{12} W). That is an interesting result because the difference between the June and annual estimates of heat flux through Davis Strait is the same size, i.e., 10–15 TW.

Since the heat flux through Davis Strait is northward, there is a convergence of heat in the volume between that line and AR7W equal to about 70 TW in 1996, and 45 TW in 2001 and 2003, implying a sea surface to air heat flux equal to that amount between Davis Strait and AR7W. These numbers are essentially independent of the choice of mass balance. For 1995, there is a divergence of about 10 TW, implying heat gain by the ocean: inspection of the hydrographic properties in the 1995 section shows a much smaller volume of warm, salty Irminger Water flowing northward in the eastern boundary current than is typical for the other years. This water is the source of heat for the basin to the north, and a decrease in its volume necessarily leads to a smaller (in this case, negative) ocean heat transport across AR7W. For comparison, PS2007 computed northward heat flux of 37.6 TW for their mass-conserving circulation above $\sigma_\theta = 27.8$ and offshore of the 700-m isobath,(implicitly assuming that the Davis Strait transport would cross AR7W outside these limits). It is true that the bulk of the heat fluxes quoted above occurs over that same domain. in the sections we have examined.

How do these values compare to air–sea heat fluxes integrated over the ocean surface between AR7W and Davis Strait? To examine this, we have used the global ocean heat flux product provided by the WHOI OAFlux project (http://oaflux.whoi.edu, funded by the NOAA Climate Observations and Monitoring (COM) program; Yu and Weller, 2007; Yu et al., 2008). This dataset provides net air–sea heat flux in one-degree latitude by one-degree longitude boxes (centered at half-degrees) in W m^{-2}, for both daily and monthly values. Using the monthly values, we have integrated the heat flux for the area east of 60°W, south of 64° N, and northwest of AR7W: Fig. 9 shows the monthly time series, the running annual mean of these values, the annual net flux for each year, and the ocean heat transport values computed for AR7W (with the sign inverted to match the directional sense of the air–sea heat flux, with positive downwards). Annual values range from 8 to 22 TW of heat going from the ocean into the atmosphere, much smaller than the extreme monthly values during winter and summer months. Ocean heat transport as plotted (OHT) is actually the convergence of heat in the volume between AR7W and Davis Strait for the June estimate in Table 3, assigning northward OHT of 5 TW through Davis Strait.

Except for 1995, our values all run higher than the 1990–1997 mean of 37.6 TW presented in PS2007. They estimated annual surface heat flux north of AR7W to be 15.2 TW, and though they felt this number was suspect, we calculate an overall mean surface heat flux for that period to be 17.4 TW. Clearly the springtime ocean heat transport exceeds the annual mean surface fluxes, even if, as PS2007 suggest, we consider the annual to be about 70% of the springtime value. If instead we consider mean surface heat fluxes for the period December through May, we find

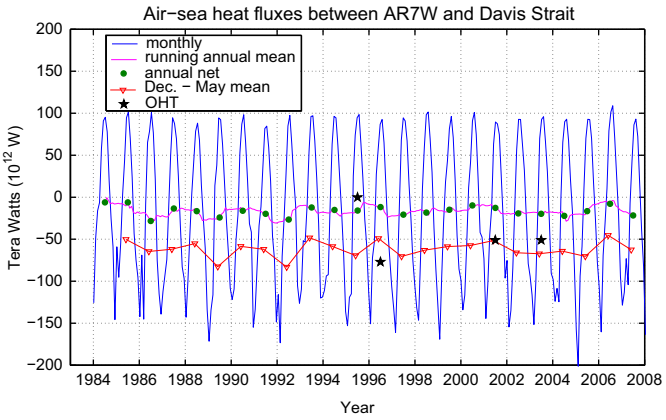

Fig. 9. Area-integrated sea-air heat flux values for a region north of AR7W from the WHOI OAFlux project (see text), and directly computed ocean heat transport values across AR7W: shown are the monthly values (blue line), the running annual mean (mauve), the annual net (green dots), the winter-spring 6-month mean (red), and individual ocean heat transport values for 4 AR7W occupations (black stars). Positive fluxes are into the ocean.

values that are similar in magnitude to our ocean heat transports, ranging from 45 to 83 TW. This correspondence suggests that the springtime AR7W sections sample the currents at a time when cold water from the winter heat loss north of AR7W is being exported southwards. Warm water parcels entering the Labrador Sea on the northeast end of the line at velocities of 10–30 cm s^{-1} would require 1–4 months to circle the perimeter of the basin and exit at the southwest end. Some of this water enters the center of the basin through instability processes, and is convected, yielding surface heat loss to the atmosphere. Although we do not know the details of how and when the cold water leaves the section, our calculations suggest that it occurs in spring; this conclusion agrees with Brandt et al. (2007)'s finding that transformed water is rapidly exported away from the region.

During the summer months, surface heat fluxes are *into* the ocean, so substantial oceanic heat storage must occur during that time. For example, the mean surface flux for June is about 91 TW into the ocean over the area in question, which is around 5×10^{11} m^2. Over a month's time, a 91 TW heat flux could heat a 100-m thick layer over this entire area by about 1 °C. The additional heat being transported by the ocean across AR7W into the volume implies some additional heat storage, but clearly it is not difficult to account for the heat being transported across AR7W.

Away from the boundary currents, the circulation derived from the inverse calculations mostly moves around water that maintains similar temperatures as it flows north or south across AR7W. If we look at how much heat is carried by each of the 6 density layers, we find that for the bottom 3 layers ($\sigma_\theta > 27.74$) the net heat flux is small compared to that carried by the top 3 layers. Furthermore, although the interior contributions in the upper 3 layers are not negligible, the bulk of the heat transport is due to the boundary currents, and specifically is associated with the Irminger Water, which is consistent with previous studies, discussed above, that use different approaches to examine heat flux in the Labrador Sea.

5. Discussion

The Labrador Sea influences the greater ocean circulation through export of locally formed water masses and modification of the boundary current system as it rounds the basin. It is therefore important to understand the role of atmospheric forcing mechanisms that affect these aspects, particularly at interannual to decadal time scales, which are relevant to climate prediction. A number of authors have examined the relationship of the North Atlantic Oscillation (NAO) to different aspects of Labrador Sea variability, with assorted conclusions.

Hurrell and Deser (2009) claimed to find that interdecadal changes in the strength of winter convection in the northern North Atlantic are synchronized with variations in the NAO. However, other authors (e.g., Khatiwala et al., 2002) seem to agree that at longer time scales (interannual, decadal), while the NAO does indeed influence winter convection, it is also necessary to include the oceanic "memory," or preconditioning, crucial to deep water formation. This is the result of the ocean integrating atmospheric forcing over a number of years. Lohmann et al. (2009) invoked a similar dynamic to explain an observed weakening of the subpolar gyre in the mid-1990s. Furthermore, Yashayaev (2007) pointed out that what appears to be a high correlation between the NAO and the air–sea heat flux in the Labrador Sea is "largely a result of the low frequency shift in the atmospheric conditions between the 1960s and early 1990s." He also noted that correlations of convection with the NAO do not persist at shorter time scales. In our work, we have too few samples of ocean heat transport crossing AR7W to draw connections with forcing mechanisms in any meaningful way. The convergence of heat in the oceanic volume between AR7W and Davis Strait is expected to compensate the loss of heat from the ocean to the atmosphere, but these surfaces fluxes vary dramatically over a year, and heat storage is a key component of the balance, as discussed by Yashayaev and Loder (2009). It is not surprising that Straneo (2006) could not find a correlation between regional heat convergence and surface fluxes, since that balance is expected to obtain over larger geographic scales, as we consider here. Even though the AR7W sections are a snapshot in time, they provide some guidance concerning the expected value of ocean heat transport across AR7W, and how it might be related to the surfaces fluxes occurring in previous months.

Other authors have considered the link between Labrador Current transport and the NAO. Han et al. (2010), using satellite data in combination with hydrography, found a correlation between Labrador Current transport anomalies and the winter NAO index at "essentially zero lag." They found a 6 Sv decline in the transport in 1996, followed by a 3 Sv recovery in the early 2000s, which we do not. However, they used the synoptic AR7W hydrographic data as a proxy for the seasonal mean, when combining it with the altimetry. Such an assumption might not be appropriate, given the intraseasonal variability found by Fischer et al. (2004, 2010), with a strong peak at periods of 10–20 days, i.e., more or less the time frame over which the data are collected.

This paper is a first attempt to investigate the interannual variability of the transports crossing AR7W from direct velocity measurements. There are marked differences in the velocity field from year to year, especially in the boundary current transports; but, as we have noted, shorter-term variability may be as large as the longer-term signal, if not larger. Sustained long-term velocity measurements would be required to separate the short- and long-term variability, as Fischer et al. (2010) have done in the DWBC. On the other hand, our composite section appears to be a reasonable representation of the (springtime) mean, if we compare our boundary current results with those calculated by other authors based on longer time series composed from both direct and indirect current measurements; the qualitative structure of the velocity field is strikingly similar to that of Pickart and Spall (2007), but our absolute velocities are stronger and the horizontal gradients sharper.

One of the central results of our work is the discovery that velocity along AR7W is dominated by top to bottom bands of unidirectional flow. Geostrophic velocity calculations therefore require an absolute velocity measurement for reference, since there is no level of no motion: complementary LADCP data are well-suited to this. Fischer et al. (2004) had found this result in the western boundary current, and we have extended it to the entire AR7W section. In addition, because the direction of flow generally changes little with depth, data from the vessel-mounted ADCP might be useful for filling in the velocity field between deep CTD/LADCP stations, though the deep LADCP measurements are superior for referencing the geostrophic velocity. In both boundary currents, steep bottom topography presents a challenge when one tries to calculate transports: finer station spacing would address this problem, as well as help to resolve the dual core of the Labrador Current at the southwestern end, and the location of the recirculation at the northeastern end.

The discovery of the bottom current along the NAMOC makes additional direct velocity measurements obtained there with both shipboard and moored instrumentation an imperative: indeed, it would be a good location for a process study to determine how overflow water property signals propagate through the Labrador Sea.

Scientists at BIO in Dartmouth (Nova Scotia, Canada) continue to occupy the AR7W section annually, now using their own LADCP. The continuity of this program over the last 20 years has provided a database that has contributed to our understanding of the Labrador Sea circulation. In this paper, we have specifically examined ocean heat transport and boundary current variability. Going forward, it is important to recognize that water mass changes, which both reflect and can have an effect on climatic changes, also occur over decadal-range periods. Yashayaev (2007), for example, used almost 50 years of hydrographic data in the Labrador Sea to examine the evolution of properties in the LSW. A warm and salty regime characterized the late 1960s and early 1970s, giving way to a colder, fresher regime in the late 1980s and early 1990s, which in its turn is being replaced by warmer and more saline conditions (Yashayaev and Loder, 2009).

The utility of satellite observations continues to expand to new applications, such as studying high frequency variability of the boundary currents and also of the central region of the Labrador Sea. Such measurements are useful for separating the low frequency changes in current transport related to subpolar gyre strength, for example, from shorter term changes, including those associated with mesoscale eddies. However, it is still crucial to have some direct velocity measurements, like the LADCP data, for both ground-truthing the remote sensing data and in-depth studies of oceanic features, phenomena and processes. Since our climate is not in a steady state, it behooves us to maintain such observational networks, which can measure water characteristics and current transports on an ongoing basis, because they may be harbingers of future changes.

Acknowledgments

The authors would like to thank the many individuals from the Ocean Sciences Division of Fisheries and Oceans Canada, at the Bedford Institute of Oceanography, as well as the Woods Hole Oceanographic Institution whose enthusiastic cooperation has made the collection of this dataset possible. We especially thank the crew of the C.C.G.S. Hudson, and many BIO technicians, including Murray Scotney, Rick Boyce and Adam Hartling, who help to mount/install, maintain and on several occasions repair the LADCP instrument package both on shore and while at sea. We also thank John Lazier, Allyn Clarke, John Loder and Glen Harrison, who have provided leadership and co-leadership of the DFO deep-ocean climate and ecosystem monitoring program since the start of the annual hydrographic, tracer and biological survey of the Labrador Sea's AR7W line.

We thank Jules Hummon (University of Hawaii) and Frank Bahr (WHOI) for their assistance with CODAS software and Yuri Geshelin (BIO) for his help with VMADCP data processing.

We would like to acknowledge Robert Pickart for initiating the collection of LADCP data on these cruises. He provided the impetus to send one of us (D. Torres) with the LADCP on the first of these joint CTD/LADCP sections in 1995. Most of the LADCP data collected and used in this study was an unfunded endeavor made possible through persistence and collaboration between WHOI and BIO.

Comments and suggestions from anonymous reviewers greatly improved the final presentation.

This material is based upon work supported by the National Science Foundation under Grant No. OCE-0622640. Igor Yashayaev is supported by the ocean climate monitoring program of the Department of Fisheries and Oceans Canada.

Appendix

The smoothing scales are 20 km in the horizontal and 50 m in the vertical. We refer to the along-track distance as X, and for the most part limit our discussion to the range $X=0$–760 km (i.e., excluding the inner shelf at the southwest end: see horizontal axes in Fig. 3). In many cases, the data did not reach these limits, and we have dealt with this in several ways. For the cumulative transport curves in Fig. 4, we have limited the calculation to the range in X over which we have actual observations. To determine the boundary current transports in Table 1 directly from the LADCP data, we first note that for those sections with the best onshore coverage, velocity in the western boundary current goes to zero around $X=0$–20 km. At the eastern end, we also assume that the velocity goes to zero at $X=760$ km. Thus, we can insert a uniformly zero velocity profile at $X=0$ (or 760) before performing the objective mapping. In this way we hope to minimize the error incurred by missing part of the boundary current transport.

Bottom topography is fixed as that along the ideal AR7W line, as shown in Fig. 3, and is resolved to 1 km in the horizontal when computing volume transports.

References

Böning, C.W., Scheinert, M., Dengg, J., Biastoch, A., Funk, A., 2006. Decadal variability of subpolar gyre transport and its reverberation in the North Atlantic overturning. Geophys. Res. Lett. 33, L21S01, http://dx.doi.org/10.1029/2006GL026906, L21S01.

Brandt, P., Funk, A., Czeschel, L., Eden, C., Böning, C.W., 2007. Ventilation and transformation of Labrador Sea water and its rapid export in the deep Labrador Current. J. Phys. Oceanogr. 37, 946–961, http://dx.doi.org/10.1175/JPO3044.1.

Chough, S.K., Hesse, R., 1980. The Northwest Atlantic Mid-Ocean channel of the Labrador Sea: III. Head spill vs. body spill deposits from turbidity currents on natural levees. J. Sediment. Petrol. 50, 227–234.

Chough, S.K., Hesse, R., Muller, J., 1987. The Northwest Atlantic Mid-Ocean channel of the Labrador Sea. IV. Petrography and provenance of the sediments. Can. J. Earth Sci. 24, 731–740.

Clarke, R.A., Gascard, J.-C., 1983. The formation of Labrador Sea Water. Part I: Large scale processes. J. Phys. Oceanogr. 13, 1764–1788.

Cuny, J., Rhines, P., Kwok, R., 2005. Davis Strait volume, fresh- water and heat fluxes. Deep-Sea Res. I 52, 519–542, http://dx.doi.org/10.1016/ j.dsr.2004.10.006.

Curry, B., Lee, C.M., Petrie, B., 2011. Volume, freshwater, and heat fluxes through Davis Strait, 2004–2005. J. Phys. Oceanogr. 41, 429–436, http://dx.doi.org/10.1175/2010JPO4536.1.

Dengler, M., Fischer, J., Schott, F.A., Zantopp, R., 2006. Deep Labrador Current and its variability in 1996–2005. Geophys. Res. Lett. 33, L21S06, http://dx.doi.org/10.1029/2006GL026702.

Drinkwater, K.F., 1988. On the mean and tidal currents in the Hudson strait. Atmosphere-Ocean 26 (2), 252–266.

Egbert, G.D., Erofeeva, S.Y., 2002. Efficient inverse modeling of barotropic ocean tides. J. Atmos. Oceanic Technol. 19 (2), 183–204.
Firing, E., and L. Gordon, 1990. Deep ocean acoustic doppler current profiling. Proc. IEEE Fourth Working Conf. on Current Measurements, Clinton, MD, Current Measurement Technology Committee of the Ocean Engineering Society, 192–201.
Fischer, J., Schott, F., Dengler, M., 2004. Boundary circulation at the exit of the Labrador Sea. J. Phys. Oceanogr. 34, 1548–1570.
Fischer, J., Visbeck, M., 1993. Deep velocity profiling with self-contained ADCPs. J. Atmos. Oceanic Technol. 10, 764–773.
Fischer, J., Visbeck, M., Zantopp, R., Nunes, N., 2010. Interannual to decadal variability of outflow from the Labrador Sea. Geophys. Res. Lett. 37, L24610, http://dx.doi.org/10.1029/2010GL045321.
Häkkinen, S., Rhines, P.B., 2004. Decline of subpolar North Atlantic circulation during the 1990s. Science 304, 555–559.
Hall, Mindy M., Bryden, Harry L., 1982. Direct estimates and mechanisms of ocean heat transport. Deep-Sea Res. 29 (3A), 339–359.
Hall, M.M., Joyce, T.M., Pickart, R.S., Smethie Jr., W.M., Torres, D.J., 2004. Zonal circulation across 52°W in the North Atlantic. J. Geophys. Res. 109, C11008, http://dx.doi.org/10.1029/2003JC002103.
Han, G., Tang, C.L., 1999. Velocity and transport of the Labrador Current determined from altimetric, hydrographic and wind data. J. Geophys. Res. 104, 18,047–18,057.
Han, G., Tang, C.L., 2001. Interannual variations of volume transport in the western Labrador Sea based on TOPEX/Poseidon and WOCE data. J. Phys. Oceanogr. 31, 199–211.
Han, G., Ohashi, K., Chen, N., Myers, P.G., Nunes, N., Fischer, J., 2010. Decline and partial rebound of the Labrador Current 1993–2004: monitoring ocean currents from altimetric and conductivity_temperature_depth data. J. Geophys. Res. 115, C12012, http://dx.doi.org/10.1029/2009JC006091.
Holliday, N.P., S. Bacon, J. Allen, and E.L. McDonagh (2009). Circulation and transport in the western boundary currents at Cape Farewell, Greenland. J. Phys. Oceanogr., 39, 1854-1870.
Hurrell, J.W., Deser, C., 2009. North Atlantic climate variability: the role of the North Atlantic Oscillation. Journal of Marine Systems 79, 231–244, http://dx.doi.org/10.1016/j.marsys.2008.11.026.
Joyce, T.M., Hernandez-Guerra, A., Smethie, W.M., 2001. Zonal circulation in the NW Atlantic and Caribbean from a meridional World Ocean Circulation Experiment hydrographic section at 66°W. J. Geophys. Res. 106 (C10), 22,095–22,113.
Katsman, C.A., Spall, M.A., Pickart, R.S., 2004. Boundary current eddies and their role in the restratification of the Labrador Sea. J. Phys. Oceanogr. 34, 1967–1983.
Kieke, D., Rhein, M., 2006. Variability of the overflow water transport in the western subpolar North Atlantic, 1950–1997. J. Phys. Oceanogr. 36, 435–456.
Khatiwala, S., Schlosser, P., Visbeck, M., 2002. Rates and mechanisms of water mass transformation in the Labrador Sea as inferred from tracer observations. J. Phys. Oceanogr. 32, 666–686.
Lab Sea Group, 1998. The Labrador Sea deep convection experiment. Bull. Amer. Meteor. Soc. 79, 2033–2058.
Lavender, K.L., Davis, R.E., Owens, W.B., 2000. Mid-depth recirculation observed in the interior Labrador and Irminger Seas by direct velocity measurements. Nature 407, 66–69.
Lazier, J., Hendry, R., Clarke, A., Yashayaev, I., Rhines, P., 2002. Convection and restratification in the Labrador Sea, 1990–2000. Deep-Sea Res., Part I 49, 1819–1835.
Lazier, J.R.N., Wright, D.G., 1993. Annual velocity variations in the Labrador Current. J. Phys. Oceanogr. 23, 659–678.
Lilly, J.M., Rhines, P.B., Schott, R., Lavender, K., Lazier, J., Send, U., D'Asaro, E., 2003. Observations of the Labrador Sea eddy field. Prog. Oceanogr. 59, 75–176, http://dx.doi.org/10/1016/j.pocean.2003.08.013.
Lohmann, K., Drange, H., Bentsen, M., 2009. A possible mechanism for the strong weakening of the North Atlantic subpolar gyre in the mid-1990s. Geophys. Res. Lett. 36 , http://dx.doi.org/10.1029/2009GL039166, L15602.
Myers, P.G., Kulan, N., Ribergaard, M.H., 2007. Irminger Water variability in the West Greenland Current. Geophys. Res. Lett. 34, L17601, http://dx.doi.org/10.1029/2007GL030419.
Pickart, R.S., Spall, M.A., 2007. Impact of Labrador Sea convection on the North Atlantic meridional overturning circulation. J. Phys. Oceanogr. 37, 2207–2227.
Pickart, R.S., Torres, D.J., Clarke, R.A., 2002. Hydrography of the Labrador Sea during active convection. J. Phys. Oceanogr. 32, 428–457.
Straneo, F., 2006. Heat and freshwater transport through the central Labrador Sea. J. Phys. Oceanogr. 36, 606–628.
Thurnherr, A.M., 2010. A practical assessment of the errors associated with full-depth LADCP profiles obtained using teledyne RDI workhorse acoustic doppler current profilers. J. Atmos. Oceanic Technol. 27, 1215–1227.
Visbeck, M., 2002. Deep velocity profiling using lowered acoustic doppler current profilers: bottom track and inverse solutions. J. Atmos. Oceanic Technol. 19, 794–807.
Yashayaev, I., 2007. Hydrographic changes in the Labrador Sea, 1960–2005. Prog. Oceanogr. 73, 242–276, http://dx.doi.org/10.1016/j.pocean.2007.04.015.
Yashayaev, I., Bersch, M., van Aken, H.M., 2007. Spreading of the Labrador Sea water to the Irminger and Iceland basins. Geophys. Res. Lett. 34, L10602, http://dx.doi.org/10.1029/2006GL028999.
Yashayaev, I., Dickson, R.R., 2008. Transformation and fate of overflows in the northern North Atlantic, in Arctic-Subarctic Ocean Fluxes. In: Dickson, R.R., Meincke, J., Rhines, P. (Eds.), Defining the Role of the Northern Seas in Climate. Springer, New York, pp. 505–526.
Yashayaev, I., Loder, J.W., 2009. Enhanced production of Labrador Sea water in 008. Geophys. Res. Lett. 36, L01606, http://dx.doi.org/10.1029/2008GL036.
Yu, L., Weller, R.A., 2007. Objectively analyzed air–sea heat fluxes (OAFlux) for the global ocean. Bull. Am. Meteorol. Soc. 88 (5), 527–539.
Yu, L., J. Xin, and R.A. Weller, 2008: Multidecade Global Flux Datasets from the Objectively Analyzed Air–Sea Fluxes (OAFlux) Project: Latent and Sensible Heat Fluxes, Ocean Evaporation, and Related Surface Meteorological Variables. Woods Hole Oceanographic Institution, OAFlux Project Technical Report. OA-2008-01, 64 pp. Woods Hole. Massachusetts.